



LAWRENCE
LIVERMORE
NATIONAL
LABORATORY

Fuel-rich Oxidation of Gasoline Surrogate Components in an Atmospheric Flow Reactor

S. Suzuki, W. J. Pitz

November 6, 2023

Combustion and Flame

Disclaimer

This document was prepared as an account of work sponsored by an agency of the United States government. Neither the United States government nor Lawrence Livermore National Security, LLC, nor any of their employees makes any warranty, expressed or implied, or assumes any legal liability or responsibility for the accuracy, completeness, or usefulness of any information, apparatus, product, or process disclosed, or represents that its use would not infringe privately owned rights. Reference herein to any specific commercial product, process, or service by trade name, trademark, manufacturer, or otherwise does not necessarily constitute or imply its endorsement, recommendation, or favoring by the United States government or Lawrence Livermore National Security, LLC. The views and opinions of authors expressed herein do not necessarily state or reflect those of the United States government or Lawrence Livermore National Security, LLC, and shall not be used for advertising or product endorsement purposes.

Fuel-rich Oxidation of Gasoline Surrogate Components in an Atmospheric Flow Reactor

Shunsuke Suzuki^{a, 1}, William J. Pitz^{b, 2}

^aResearch Institute for Energy Conversion, National Institute of Advanced Industrial Science and Technology (AIST), 1-2-1 Namiki, Tsukuba 305-8564, Japan

^bMaterials Science Division, Lawrence Livermore National Laboratory, Livermore, CA 94551, USA

¹ S. Suzuki, email: suzuki-shunsuke.cv@aist.go.jp

² W. J. Pitz, email: pitz1@llnl.gov

ABSTRACT

Fuel-rich oxidation of three typical gasoline surrogate components, toluene, iso-octane, and n-heptane, was investigated in an atmospheric-pressure flow reactor at mean gas temperatures from 1050 to 1350 K, equivalence ratio of 9.0, and residence times of 0.45 and 1.2 s. Not only polycyclic aromatic hydrocarbons (PAHs) up to 3 ring structure but also small intermediate products from C₁ to C₅ were quantified by a gas chromatograph mass spectrometry coupled with photon ionization and gas chromatograph with flame ionization detector, respectively. The kinetic model recently developed by Lawrence Livermore National Laboratory was revised to reflect the results of many recent investigations. Basically, the updated model could satisfactorily reproduce the experimental mole fractions of many species. The experimental and simulated results showed that PAH mole fractions produced were in the order of toluene, iso-octane, and n-heptane. The kinetic analysis using the model was carried out to explore PAH formation pathways, especially focusing on naphthalene, acenaphthylene, and phenanthrene. Through rate of production analysis, it was found that the main formation pathways of many PAHs were affected by the fuels. Although resonantly stabilized radicals, such as benzyl and fulvenallenyl radicals, played a crucial role in the formation pathways of many PAHs in every fuel, they were produced through hydrogen elimination of toluene in toluene fuel, while they were formed from small intermediate products in iso-octane and n-heptane fuels. Sensitivity analysis revealed the difference and similarity of the reactions with large positive coefficients

according to the fuels studied here. The molecular growth reactions of aromatic species were influential in PAH production in every fuel, whereas the ring formation reactions from small species and the reactions involving toluene had large positive sensitivity coefficients in iso-octane/n-heptane and toluene fuels, respectively.

Key Words: Polycyclic aromatic hydrocarbon (PAH); flow reactor; toluene; n-heptane; iso-octane; fuel-rich oxidation

1. INTRODUCTION

Soot particles emitted from internal combustion engines are serious issues for environment and human health [1], thereby stringent regulations have been proposed around the world to restrict soot emissions from automotive transport sector. Among gasoline engines, the importance of gasoline direct-injection (GDI) engines are increasing owing to higher fuel economy compared with conventional port fuel injection (PFI) engines. However, GDI engines are suffering from more soot emissions than PFI engines, particularly during the cold start phase and stratified operation [2]. Polycyclic aromatic hydrocarbons (PAHs) are known as precursors of soot particles and have an essential role in soot formation processes [3]. Thus, to suppress the soot production in GDI engines, a fundamental understanding of PAH formation processes in gasoline fuels is required.

Practical gasoline fuels are complex mixtures of a variety of hydrocarbons. In addition to hydrocarbons, market gasoline fuels often contains ethanol, but its effect is not considered, however the effect of methanol was considered in a previous study [4]. Hydrocarbons contained in gasoline fuel can be categorized according to their molecular structure, such as normal, branched, and cyclic alkanes, linear alkenes, and aromatics [5]. Thus, surrogate fuels consisting of a limited number of pure components have been employed to capture similar physical and chemical properties and combustion characteristics of complex real fuels. As gasoline surrogate fuels, binary mixtures of n-heptane and iso-octane denoted as primary reference fuels (PRFs), and ternary mixtures of toluene, n-heptane, and

iso-octane known as toluene primary reference fuels (TPRFs) have been widely formulated [6]. Toluene, n-heptane, and iso-octane represent aromatics, linear alkanes, and branched alkanes, respectively. In addition to fundamental studies on the laminar burning velocity [7] and ignition delay time [8] using TPRFs, experimental investigations of soot and PAH formation by TPRFs have been performed using flames [9,10,11,12,13], jet-stirred reactor (JSR) [14,15], and flow reactor [14], to deeply understand the combustion characteristics of gasoline fuels. Park et al. [10], Hua et al. [11] and Liang et al. [12] qualitatively measured the PAH formation of gasoline surrogates using laser-induced fluorescence technique, as well as laser-induced incandescence for measuring soot volume fraction. Shao et al. [14,15] studied the pyrolysis of gasoline surrogates using JSR coupled with gas chromatography (GC) with a flame ionization detector (FID) and found that TPRFs produced more PAHs than PFRs because toluene was included in TPRFs. Shao et al. [14] analyzed the PAH mole fractions formed in pyrolysis of gasoline surrogates in a flow reactor coupled with synchrotron vacuum ultraviolet photoionization molecular beam mass spectrometry and showed that production of small PAHs, such as benzene and naphthalene, were slightly higher in TPRF with research octane number (RON) of 70 than that with RON of 97.5, while the latter fuel produced slightly higher phenanthrene and pyrene. Despite many efforts so far, there are still limited studies to quantitatively evaluate PAH formation in fuel-rich oxidation of TPRFs. Therefore, to enhance the understanding of PAH formation mechanism in gasoline and to underline the effect of hydrocarbons with different molecular structures

on PAH formation chemistry, fuel-rich oxidation of TPRF components, such as toluene, iso-octane, and n-heptane, should be investigated.

The objective of this study is to examine fuel-rich oxidation of gasoline surrogate components, toluene, iso-octane, and n-heptane, using a flow reactor at atmospheric pressure, mean gas temperatures from 1050 to 1350 K, equivalence ratio of 9.0, and residence times of 0.45 and 1.2 s. In addition to PAHs from monocyclic to tricyclic structures, small intermediate species from C₁ to C₅ produced during fuel oxidation were quantified. Small intermediate species, such as acetylene, allene, their derivative radicals, and others, are important because they are building blocks in PAH growth reactions [16,17,18]. The mole fractions of PAHs were evaluated by a GC mass spectrometry (GC-MS) coupled with photon ionization, while small intermediate species were quantified using GC-FID. A chemical kinetic model which was recently developed by Lawrence Livermore National Laboratory (LLNL) was updated according to various studies and employed to reproduce the experimental results obtained in a flow reactor. Computed and measured concentration profiles of species were compared to evaluate the modeling performance. Kinetic analysis using the model was carried out to clarify the fuel-specific reaction pathways of various PAHs.

2. EXPERIMENTAL AND ANALYTICAL METHODS

2.1. Reactor system

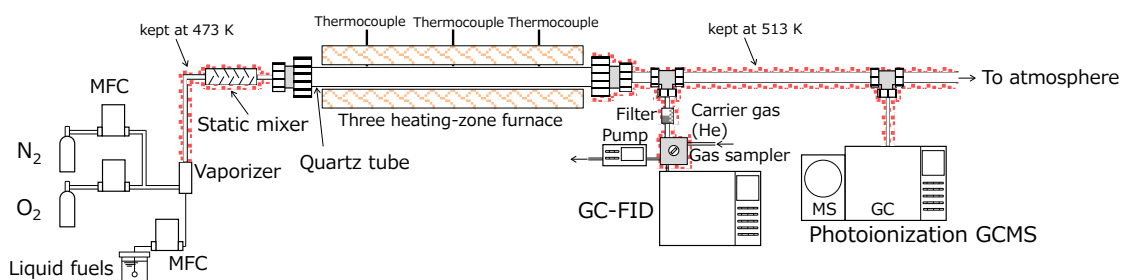


Fig. 1 Depiction of experimental apparatus in this study.

The overall experimental apparatus in this study is depicted in Fig. 1. This apparatus consists of several units, such as a feedstock supply/control unit, flow reactor, and sample system for analysis. Because the same feedstock supply/control unit and flow reactor as previously reported [19] are used, a brief explanation is given here.

Liquid fuels, such as toluene (>99.8%, FUJIFILM Wako Pure Chemical Corporation), iso-octane (>99.0%, Tokyo Chemical Industry Co., Ltd.), and n-heptane (>99.0%, FUJIFILM Wako Pure Chemical Corporation), were supplied to a vaporizer via fuel reservoir and mass flow controller (MFC). In a vaporizer, liquid fuels were mixed with oxygen (>99.999%, Taiyo Nippon Sanso Corporation) and nitrogen (>99.99995%, Taiyo Nippon Sanso Corporation) whose flow rates were adjusted by individual mass flow controllers, and then the mixtures were introduced into a reactor. The temperature of feeding lines from an outlet of vaporizer to a reactor inlet was kept at 473 K to avoid condensation of the vaporized fuels. The mole fraction of oxygen at a reactor inlet was fixed at 0.600 vol.% under a standard condition. The concentrations of toluene, iso-octane, and n-heptane at a reactor inlet were 0.600, 0.432, and 0.491 vol.% so that equivalence ratio was 9.0. Nitrogen was used as balance gas and

its concentration at a reactor inlet accounted for more than 98.8 vol.%.

The reactor consists of a quartz tube of 10 mm inner diameter and 1050 mm length, which was placed in a three heating-zone furnace, where the temperature of each zone of a furnace was separately controlled by R-type thermocouples, enabling the uniform temperature profile. The detailed information on reactor features used in this study can be found in our previous paper [19]. The temperature was varied from 1050 to 1350 K and the residence time, which was adjusted by a total gaseous flow rate, was 0.45 and 1.2 s. The measurements at a temperature lower than 1000 K were not performed because PAH production was the focus in this study and expected to be small at a low temperature. Formation of carbonaceous deposits could be found on the inner wall of the reactor tube after experiments. To avoid any effect of the deposits on the measurements, oxygen diluted with nitrogen was fed to the reactor to burn the deposits before conducting the experiments. The carbon balance was evaluated in our previous paper [19], showing that it deteriorated at elevated temperatures. This may be attributed to the formation of large molecular weight species, such as carbonaceous deposits stated above.

2.2. Sampling system

GC-FID (Shimadzu GC-2014) was employed for quantifying C₁–C₅ hydrocarbons included in sampled gas. Since the sampling system using GC-FID was described in detail previously [19], a short

description is provided here. Quantified species were methane, acetylene, ethylene, allene (propadiene), propyne (methylacetylene), propylene (propene), vinylacetylene, 1,3-butadiene, and cyclopentadiene. Pure He (>99.99995 %) was used as carrier gas for the GC-FID. TC-BOND Alumina/KCl with an inner diameter of 0.25 mm, length of 30 m, and film thickness of 4 μm was employed as a capillary column for separation of gaseous species. Gaseous species from C_1 – C_4 were directly calibrated by means of commercially available standard gases diluted with nitrogen. On the other hand, the mole fraction of cyclopentadiene was indirectly evaluated using the calibration results of other gases because signal intensities of hydrocarbons are nearly proportional to carbon numbers included in the species in an FID system. Detailed information, such as operation procedure of GC, is available in our previous paper [19]. The lower detection limit of species in GC-FID system was approximately 0.1 ppm. Uncertainty analysis was conducted previously [19], showing that total uncertainty correlated with present GC-FID was estimated to be less than 15% for all analyzed small intermediate species. Experimental data of small species in toluene fuel at residence time of 1.2 s were obtained in our previous study [19], while other data were newly measured in this study.

Photon ionization GC-MS (PI GC-MS, JEOL JMS-Q1050GC) was newly developed in order to quantify PAHs included in sampled gas. Mass spectrometry coupled with photon ionization is a powerful tool and has widely been applied to combustion investigations to provide advances in combustion chemistry [20,21,22]. Although electron ionization is another technique frequently used

in combustion studies [23,24], it involves fragmentation of gaseous species, which often leads to difficulties in identifying chemical species. One of advantages related to photon ionization method is soft ionization of species, which is able to minimize fragmentation of PAHs. A deuterium lamp which was embedded in a mass detection unit was employed to generate vacuum ultraviolet light with fixed energy of 10.3 eV which is sufficient to ionize PAHs. A capillary silica tube with inert treatment was used as a resistance tube in our PI GC-MS so that the pressure in a mass spectrometer is kept at a suitable level for analysis. Note that silica tube does not have separation function of species. In general, the signal intensity with specific mass-to-charge ratio (m/z), $S_{m/z}$, can be expressed as follows [21].

$$S_{m/z} \propto X_{m/z} \times \sigma_{m/z} \times D_{m/z} \times \phi \times \lambda \quad (1)$$

where $X_{m/z}$ represents the mole fraction of the species at specific m/z , $\sigma_{m/z}$ is photoionization cross section, $D_{m/z}$ is a mass discrimination factor, ϕ signifies photon flux, and λ is a sampling function.

In our study, because the temperature and pressure in a mass detection unit can be assumed to be nearly constant, it is reasonable to consider that ϕ and λ are independent of experimental conditions.

Hence, from equation (1), the following equation can be derived when $m/z = 78$ which corresponds to benzene is used as a reference material.

$$X_{m/z} = X_{Benz} \times \frac{S_{m/z}}{S_{Benz}} \times \frac{\sigma_{Benz}}{\sigma_{m/z}} \times \frac{D_{Benz}}{D_{m/z}} \quad (2)$$

The rationality whether the signal intensity at $m/z = 78$ can be treated as that of benzene is worth discussing. Figure S1 in the supplementary material shows that experimentally quantified benzene

mole fractions were in remarkable agreement between PI GC-MS and GC-FID, where GC-FID was regarded as a benchmark because GC-FID is a reliable equipment for quantification of hydrocarbons [19]. This result strongly indicates that it is reasonable to treat the signal intensity at $m/z = 78$ in PI GC-MS as that of benzene. Equation (2) can be further transformed for quantification of the target m/z as follows.

$$X_{m/z} = \frac{S_{m/z}}{\alpha_{Benz}} \times \frac{\sigma_{Benz}}{\sigma_{m/z}} \times \frac{D_{Benz}}{D_{m/z}} \quad (3)$$

where $X_{m/z}$ is the mole fraction of target m/z , $\alpha_{Benz} = S_{Benz}/X_{Benz}$ is the gradient of benzene calibration curve, $S_{m/z}$ is the signal intensity of target m/z , $\sigma_{m/z}$ is the photoionization cross section of target m/z , σ_{Benz} is the photoionization cross section of benzene, $D_{m/z}$ is the mass discrimination factor of target m/z , and D_{Benz} is the mass discrimination factor of benzene. The gradient of benzene calibration curve, α_{Benz} , was calculated using gaseous benzene with known concentration diluted by N_2 . Note that standard calibration materials were not used for PAHs larger than $m/z = 78$. The signal intensity of target m/z , $S_{m/z}$, was monitored during analysis and was determined by subtracting the background signal intensity from the measured one at target m/z . Although the signal intensity of specific m/z , $S_{m/z}$, was the sum of that of all isomers, the photoionization cross section and mass discrimination factor of specific m/z were basically determined based on the value of the structure with the largest production. For instance, at $m/z = 152$, acenaphthylene, 1-ethynyl naphthalene, and 2-ethynyl naphthalene are candidates as isomers. However, because the production of acenaphthylene is

expected to be the largest based on our experience and results stated later, the photoionization cross section and mass discrimination factor at $m/z = 152$ was determined based on acenaphthylene. The lists of the photoionization cross section and mass discrimination factor reflecting several preceding papers [25,26,27,28] are available in Tables S1 and S2 in the supplementary material, respectively. If light energy for ionization is tunable, it is possible to record mass-specific photoionization efficiency (PIE) curves which help with isomer identification [20,29]. However, the technique to identify isomers using PIE curves is limited to small species containing less than 7 heavy atoms [20]. Hence, the use of a fixed energy light with 10.3 eV in this study is not a major barrier for PAH measurement, and we believe that the signal intensity of specific m/z , $S_{m/z}$, obtained here is beneficial for advancing the PAH chemistry. In this study, not only the m/z corresponding to major PAHs, such as 128 for naphthalene and 178 for phenanthrene/anthracene, but also that corresponding to minor PAHs, such as oxygenated PAHs (OPAHs), were analyzed, such as $m/z = 108$ and 158. During analysis, the temperatures of GC oven, interface between GC and mass spectrometer, and mass spectrometer were kept at 523 K, 483 K and 453 K, respectively. The resolution of mass ($m/\Delta m$) was higher than 2000 according to the specification of the apparatus. m/z investigated here was from 78 to 180 which corresponded to monocyclic to tricyclic structures. The lower detection limit of PI GC-MS in this study was approximately ~ 0.1 ppm. The uncertainties of obtained mole fractions using photon ionization method were precisely described elsewhere [20,21,29]. When the uncertainty analysis is

conducted in this study based on the discussions of previous papers, the accuracy of the directly calibrated species, benzene in this study, is expected to be less than $\pm 20\%$, while the uncertainty for the mole fractions of larger species than benzene can be as large as a factor of 2–4 because the photoionization cross sections and mass discrimination factors were estimated. Note that in the present conditions, the concentrations of iso-octane and n-heptane in sampled gas were lower than the detection limit in both GC-FID and PI GC-MS, meaning that almost all of iso-octane and n-heptane were converted.

3. NUMERICAL APPROACH

A detailed kinetic model developed by LLNL [4] was employed as a base one. This model contains detailed PAH growth reactions up to five rings and consists of 1328 species and 8006 elementary reactions [4]. The LLNL model was originally developed for describing the aromatic combustion mechanism and has been updated to incorporate molecular growth chemistry revealed by theoretical and experimental studies [30]. This model has been validated against flames involving aromatics and C₃ species [20,31], pyrolysis of gasoline surrogates in JSR [15], and fuel-rich oxidation of ethylene, toluene, n-decane, and toluene/methanol in a flow reactor [4,19,32]. Although the previous model could basically reproduce the experimental data of many PAHs well, there were some discrepancies between the simulated and experimental results in several PAHs, such as naphthalene and

acenaphthylene in [4] and biphenyl and fluorene in [32]. Furthermore, the reaction mechanism of several OPAHs like naphthol and naphthoquinone was insufficiently developed in the previous model. We added multiple PAH formation reactions into the base model for improving the model prediction, and the main revisions on the model are stated in detail later. The updated model includes 1394 species and 8297 reactions. To compare experimental results with calculated data, one-dimensional simulations were performed using the Plug Flow Reactor (PFR) module in OpenSMOKE++ Suite [33,34]. The rationality using the PFR module was already discussed in our previous paper [19]. The temperature profiles determined in our previous study [19] were used as input data for the simulations. When comparing the measured and predicted results of PAHs in this investigation, the following point should be noted; because the measured mole fractions of PAHs larger than benzene were determined based on the signal intensity at m/z which was the sum of the signal intensities of potential isomers, calculated mole fractions were determined by the sum of those of species with the same m/z included in the kinetic model. For example, considering species at $m/z = 152$, the present model includes three isomers, acenaphthylene (A2R5), 1-ethynyl naphthalene (A2C₂H-1), and 2-ethynyl naphthalene (A2C₂HV). Thus, the calculated mole fraction at $m/z = 152$ was the sum of acenaphthylene, 1-ethynyl naphthalene, and 2-ethynyl naphthalene. Table S3 in the supplementary material shows the summary of structures and nomenclatures of isomers at similar m/z which were contained in the model and used for the simulations.

3.1. Revisions of the kinetic model

The newly added and/or modified reactions are stated in the following sections according to aromatic size.

3.1.1. C₇ aromatic species

Reactions involving toluene (C₆H₅CH₃), benzyl radical (C₆H₅CH₂), and vinyl-cyclopentadienyl radical (VCP-C₇H₇) were modified and/or added. Benzyl radical formation from propargyl radical and vinylacetylene (C₃H₃ + C₄H₄ = C₆H₅CH₂) was added according to the study by Jones et al. [35]. The rate parameters of toluene formation from 1,3-butadiene and propargyl radical (C₄H₆ + C₃H₃ = C₆H₅CH₃ + H) was referred to C₃H₃ + C₄H₄ = C₆H₅CH₂ according to JetSurf2.0 model [36]. The decomposition reaction of OC₆H₄C₂H₃ to produce vinyl-cyclopentadienyl radical and CO (OC₆H₄C₂H₃ => VCP-C₇H₇ + CO) was added and its rate constants were taken from C₆H₅O = C₃H₅ + CO included in the base model. Furthermore, the reaction block involving VCP-C₇H₇ leading to fulvenallene (C₇H₆) and indene (IND) was added by referring to several papers [18,37,38].

3.1.2. C₁₀ aromatic species

Formation reactions of naphthalene (NAPH), 1-naphthyl radical (NAPH-), and 2-naphthyl radical

(NAPHV) from benzyne ($C-C_6H_4$) and vinylacetylene were added based on the recent study by Monluc et al. [39]. The rate constants of hydrogen elimination reactions of naphthalene to produce 1-naphthyl and 2-naphthyl radicals were revised according to the same article [39]. The reaction between benzyl and propargyl radicals to produce dialin ($C_{10}H_{10}$) was added by referring to C3MechV3.3 [40].

3.1.3. C_{12} aromatic species

Methyl addition to benzo-fulvenallenyl radical ($C_9H_6-C_2H$) to produce acenaphthylene (A2R5) and 1-ethynyl naphthalene (A2C₂H-1) was described based on Jin's study [41]. Jin et al. [42] and Hamadi et al. [43] recently pointed out the importance of the combination between indenyl (C_9H_7) and propargyl radicals toward acenaphthylene production where ring expansion and hydrogen elimination take place. Though the above reaction underwent multi-step scheme in their studies [42,43], the detailed theoretical investigations of this reaction system have not yet been performed to our knowledge. Hence, we described as a global reaction ($C_9H_7 + C_3H_3 \Rightarrow A2R5 + H_2$) whose rate parameters were taken from the reaction to form 1-(propa-1,2-dien-1-yl)-1H-indene (C_9H_6VCCVC) from propargyl and indenyl radicals included in the base model. Because Jin et al. indicated that hydrogen-abstraction phenylacetylene-addition could lead to efficient formation of peri-condensed aromatic hydrocarbons [44], we explored whether the reaction pathway from phenylacetylene and 1-naphthyl radical to acenaphthylene and phenyl radical affected acenaphthylene production. However,

the above reaction scheme was not included in the present model because we found that its effect on acenaphthylene production was very minor. Biphenyl ($C_{12}H_{10}$) formation reaction from fulvenallenyl (C_7H_5) and cyclopentadienyl (C_5H_5) radicals was added as suggested by Jin's study [42], and its rate parameters were taken from the recombination of propargyl radicals to produce benzene and fulvene included in the base model.

3.1.4. C_{13} aromatic species

Fluorene, fluorenyl radical (RFLUORENE), phenalene, and cyclopenta-naphthalene (A2CYC5 and A2CYC5-L) were C_{13} aromatic species. The combination of indene/indenyl radical and cyclopentadienyl radical/cyclopentadiene (C_5H_6) leading to the production of fluorene and 1H-cyclopenta(a)naphthalene (A2CYC5) via isomerization and methyl radical removal was described in a multiple-step manner as shown by Jin et al. [42]. The reaction between benzo-fulvenallenyl radical and acetylene to form fluorenyl radical ($C_9H_6-C_2H + C_2H_2 = RFLUORENE$) was added in analogy with the reaction of fulvenallenyl radical with acetylene to form indenyl radical, and its rate parameters were referred to the study by Matsugi and Miyoshi [45]. The reaction block involving methyl-biphenyl (ME- $C_{12}H_9$) and methyl-biphenylyl radical ($C_{12}H_9CH_2$) leading to fluorene production was described based on the recent theoretical studies [46,47]. Because the recent experimental study suggested the importance of the reactions between $C_6 + C_7$ species for fluorene production [48], we added several

reactions, such as fulvenallenyl radical with benzene/phenyl radical to form fluorene and fulvenallenyl radical + benzyne leading to fluorenyl radical. The rate constants of methyl-naphthyl radical (A2CH₂) + C₂H₂ reactions to produce phenalene, 1H-cyclopenta(a)naphthalene (A2CYC5), and 1H-cyclopenta(b)naphthalene (A2CYC5-L) were modified based on Galimova's study [46]. The reactions between 1- and 2-naphthyl radicals and allene/propyne to produce C₁₃ species were added based on the recent studies [49,50]. Unimolecular H-elimination reaction of diphenylmethane was added due to the analogy with the reaction of toluene to form benzyl radical + H.

3.1.5. C₁₄ aromatic species

In addition to diphenylacetylene formation from the combination of phenylacetylene (C₆H₅C₂H) and phenyl radical (C₆H₅) which is already incorporated in the base model, the production reaction of 9-methylene-fluorene (CH₂FLUORENE) was added (C₆H₅C₂H + C₆H₅ = CH₂FLUORENE + H), taking the rate constants of this reaction from Jin's study [51]. Their study [51] also showed the pathway from 1,2-diphenylvinyl radical (C₁₄H₁₁) to phenanthrene plus H (C₁₄H₁₁ = PHNTHRN + H) and this pathway was added to the present model. C₉H₆-C₅H₅ radical produced through the combination of indenyl and cyclopentadienyl radicals underwent hydrogen elimination to produce benzofulvalene (C₉H₆-C₅H₄) whose rate parameters were referred to H-elimination of fulvalenyl radical to produce fulvalene shown in [52]. Benzofulvalene further underwent H-assisted isomerization to produce

phenanthrene and anthracene according to the study by Krasnoukhov et al. [53].

3.1.6. Oxygenated aromatic species

The reaction block involving benzofuran and dibenzofuran formation was refined based on our previous investigation [32]. The reaction mechanism involving 1,2-naphthoquinone (O-OA2O), 1,4-naphthoquinone (P-OA2O), and naphthol (NAPHOH) was updated in this study. The reactions of 2-naphthyl radical with O₂ and naphthoxy radical (NAPHO) with O to produce 1,2-naphthoquinone were added in analogy with those of phenyl and phenoxy radicals as shown in Morozov's study [54]. Similarly, the reactions from 1-naphthyl and naphthoxy radicals with O₂ and O, respectively, to form 1,4-naphthoquinone were referred to the reactions involving phenyl and phenoxy radicals [55]. Also, naphthoxy radical reacted with O₂ to produce 1,2-naphthoquinone and 1,4-naphthoquinone, taking the rate constants of these reactions from benzoquinone formation from phenoxy radical + O₂ included in the base model. The rate parameters of decomposition of 1,2-naphthoquinone and 1,4-naphthoquinone to produce indenone (C₉H₆O) and CO were adopted from O-C₆H₄O₂ = C₅H₄O + CO in the base model. The reaction mechanism involving naphthalene and O to form naphthol was newly added based on the reaction scheme of benzene + O leading to phenol which is described in the base model.

4. RESULTS AND DISCUSSIONS

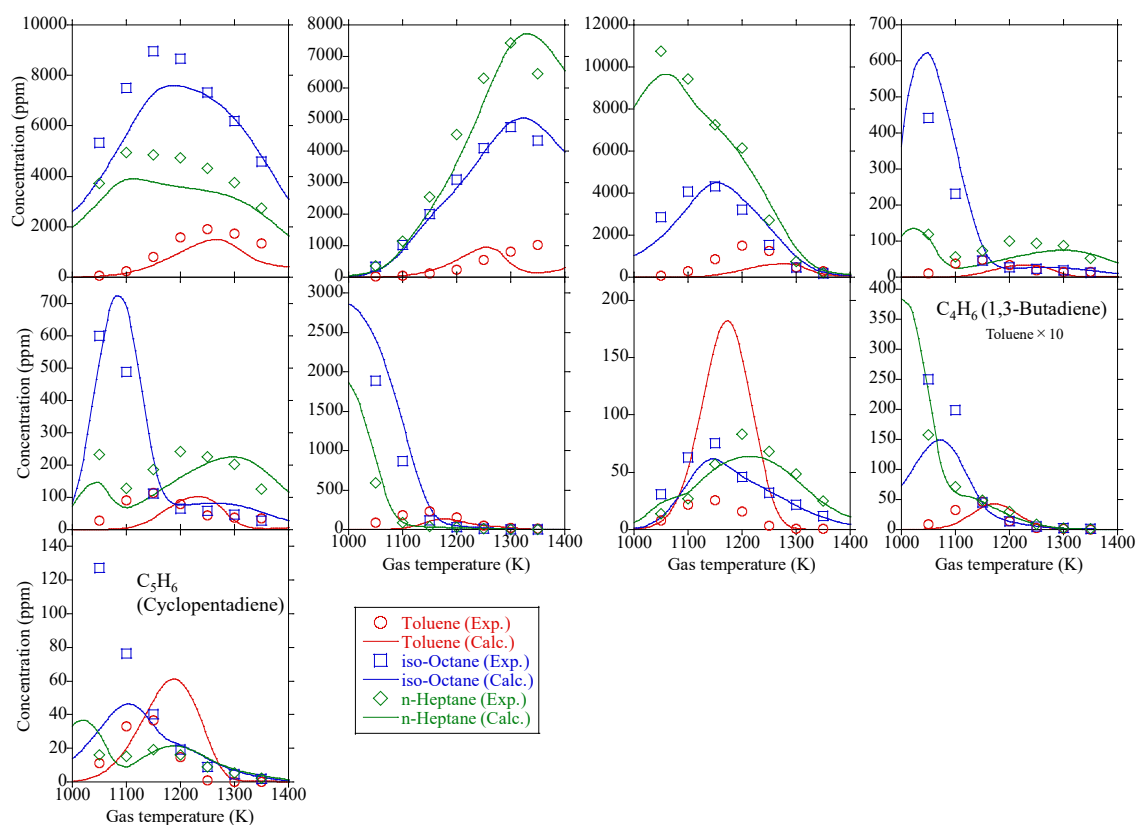


Fig. 2 Concentration profiles of small intermediate species in fuel-rich oxidation of toluene, iso-octane, and n-heptane as a function of temperature. Equivalence ratio and residence time were 9.0 and 1.2 s, respectively. Symbols are experimental data; lines are simulated profiles.

5. Experimental and simulated results of small intermediate species as a function of gas temperature

In this section, the experimental and simulated results of small intermediate products produced during oxidation of fuels at a residence time of 1.2 s are provided in Fig. 2. The results at a residence time of 0.45 s are given in Fig. S2 in the supplementary material. Note that measured and calculated data of several species, e.g., allene in toluene and n-heptane fuels and 1,3-butadiene in toluene fuel, were multiplied so that concentration profiles can be visible. Although Figs. 2 and S2 show similar tendency, the shape of species profiles in Fig. 2 shifts approximately 50 K to the low temperature side compared

with that in Fig. S2, suggesting that the effect of residence time is not so large in the range of this study. Figures 2 and S2 show that the current model could satisfactorily capture the experimental tendency. As for C₁ and C₃ species, iso-octane produced the largest amount, followed by n-heptane and toluene, while the largest concentrations of C₂ species were acquired in n-heptane, followed by iso-octane and toluene. Although 1,3-butadiene production in toluene fuel was much lower than that in iso-octane and n-heptane, production of vinylacetylene and cyclopentadiene was similar between fuels. Since acetylene, allene, propyne, vinylacetylene, and cyclopentadiene, including derivative radicals from these species, are important for PAH growth [16,18,37,38,39,45], the main reaction pathways of these products were analyzed using the model. Regarding acetylene, decomposition of cyclopentadienone ($C_5H_4O \Rightarrow 2C_2H_2 + CO$) produced from HCO elimination of C₆H₅OO was dominant in toluene fuel at 1300 K. It is noted that in Fig. 2 the simulated acetylene concentration increases rapidly with increasing temperature and then decreases, while the measured values increase more slowly. This disagreement could be due to an assumption in the cyclopentadienone decomposition reaction above that two C₂H₂ are formed from a rapid decomposition of CYC₄H₄ (cyclobutadiene). This assumption was made because cyclobutadiene is expected to be short-lived [56] and a cyclobutadiene kinetic submodel is not available (to the author's knowledge) to simulate its consumption. Future development and inclusion of a cyclobutadiene submechanism may be needed to improve the acetylene agreement. In iso-octane and n-heptane fuels at 1300K, sequential H-

elimination of ethylene ($C_2H_4 + H = C_2H_3 + H_2$ and $C_2H_3 (+M) = C_2H_2 + H (+M)$) was dominant for acetylene formation. In addition, H-assisted propyne decomposition ($C_3H_4-P + H = C_2H_2 + CH_3$) was important in iso-octane fuel. As for allene, although H-elimination of C_3H_5-A ($C_3H_5-A = C_3H_4-A + H$) was dominant in toluene and n-heptane fuel at 1300 K, C_3H_5-A was produced from $C_5H_6 + H = C_3H_5-A + C_2H_2$ and sequential H-elimination of propylene (C_3H_6) in toluene and n-heptane, respectively. On the other hand, the decomposition of IC_4H_7 ($IC_4H_7 = C_3H_4-A + CH_3$) which was primarily formed by hydrogen abstraction reaction of isobutene (IC_4H_8) was main production pathway of allene in iso-octane fuel. Propyne was mainly produced from isomerization of allene ($C_3H_4-A = C_3H_4-P$ and $C_3H_4-A + H = C_3H_4-P + H$) and $CH_3 + C_2H_2 = C_3H_4-P + H$ in every fuel at 1300 K. As main production pathways of vinylacetylene, H-elimination of C_4H_5-N ($C_4H_5-N = C_4H_4 + H$) produced through CO removal of cyclopentadienone ($C_5H_4O + H = C_4H_5-N + CO$) was predominant in toluene fuel at 1300 K. Figure 2 shows that the simulated vinylacetylene concentration was overestimated by a factor of 7 although the current mechanism could qualitatively capture the experimental tendency. This may be because the reaction chemistry of vinylacetylene formation from toluene is still not understood comprehensively, and further refinement of the mechanism is required for good quantitative agreement. On the other hand, H-elimination of C_4H_5-N and C_4H_5-I ($C_4H_5-N = C_4H_4 + H$ and $C_4H_5-I = C_4H_4 + H$) was important for vinylacetylene production in iso-octane and n-heptane fuels at 1300 K. In addition, $C_2H_3 + C_2H_2 = C_4H_4 + H$ was also important for vinylacetylene production in n-heptane. In our model,

cyclopentadiene (C_5H_6) was mainly formed through $H + C_3H_5$ produced from CO elimination of C_6H_5O in case of toluene at 1300 K, while dehydrogenation of cyclopentene ($CYC_5H_8 = C_5H_6 + H_2$) and cyclization of CVCCVCCJ ($CVCCVCCJ = C_5H_6 + H$) produced from hydrogen removal of 1,3-pentene were dominant pathway for cyclopentadiene formation in iso-octane and n-heptane. In this way, the production and reaction pathways of small intermediate species which can become building blocks for PAH depend on the fuels.

5.1. Experimental and simulated results of PAHs as a function of gas temperature

Figures 3 and 4 present experimental and calculated results of PAHs at a residence time of 1.2 s as a function of temperature. Major PAHs corresponding to $m/z = 78, 92, 104, 116, 128, 152, 154, 166,$ and 178 are adopted in Fig. 3 and the rest is shown in Fig. 4. The results at a residence time of 0.45 s are provided in Figs. S3 and S4 in the supplementary material. Note that the structures and nomenclature of PAH isomers considered for each m/z in the chemical kinetic model are summarized in Table S3 in the supplementary material. Measured and calculated data of several species, e.g., $m/z = 166$ in Fig. 3 and $m/z = 180$ in Fig. 4 in iso-octane and n-heptane fuels, were multiplied. Similarly to small intermediate products in Figs. 2 and S2, the shapes of profiles of most PAHs shift to the low temperature side at residence time of 1.2 s (Figs. 3 and 4) compared to those at 0.45 s (Figs. S3 and S4). In Fig. 3, PAH concentrations in toluene were overall the largest among the fuels studied here,

followed by iso-octane and n-heptane. Note that in the experiments, production of several PAHs, such as $m/z = 104$ and 116 , was larger in iso-octane than that in toluene at 1050 K. This may be due to the difference of the fuel reactivity: the conversion of toluene at 1050 K was several percent, while almost 100% of iso-octane was reacted at the same temperature. In the experimental results in Fig. 3, peaks in PAH concentration for m/z larger than 104 were observed in every fuel over the temperature range studied, however, the peak temperature presenting the maximum PAH concentration depended on the fuels: it was the lowest and highest in toluene and n-heptane, respectively, while it was located between

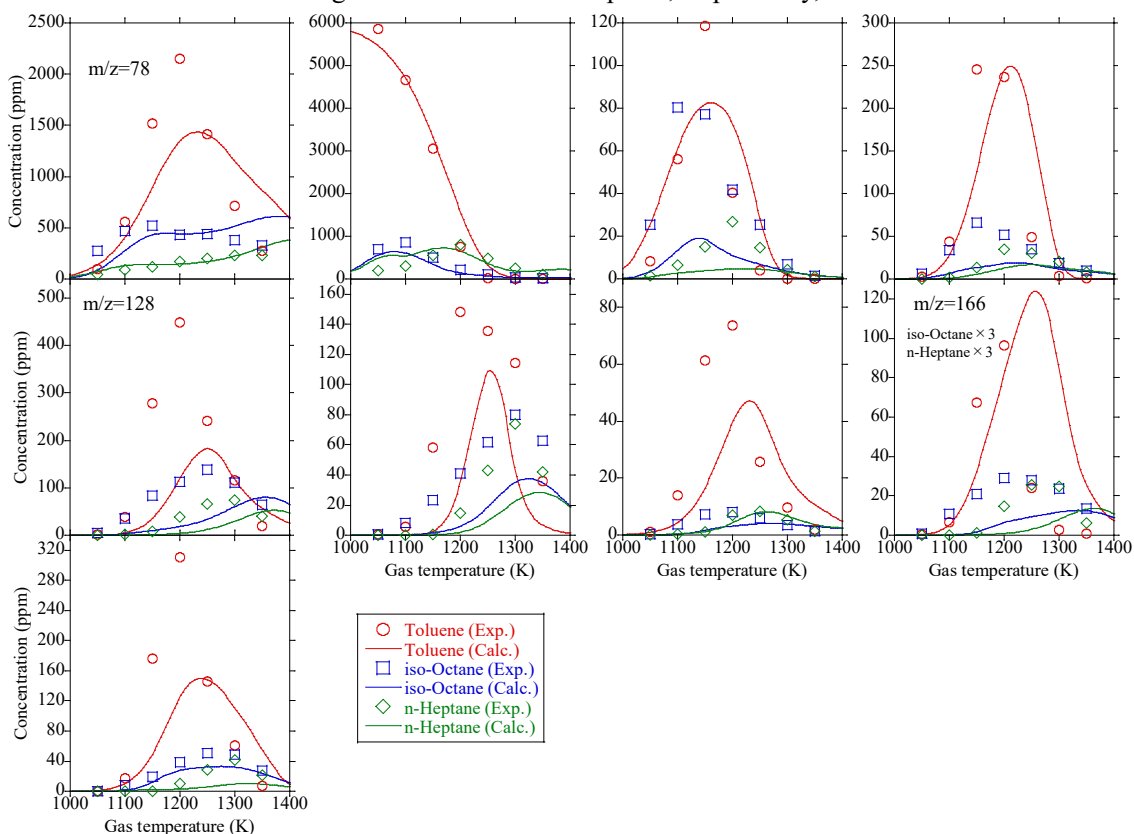


Fig. 3 Concentration profiles of PAHs corresponding to $m/z = 78, 92, 104, 116, 128, 152, 154, 166,$ and 178 in fuel-rich oxidation of toluene, iso-octane, and n-heptane as a function of temperature. Equivalence ratio and residence time were 9.0 and 1.2 s, respectively. Symbols are experimental data; lines are simulated profiles. See Table S3 for structures associated with these m/z values.

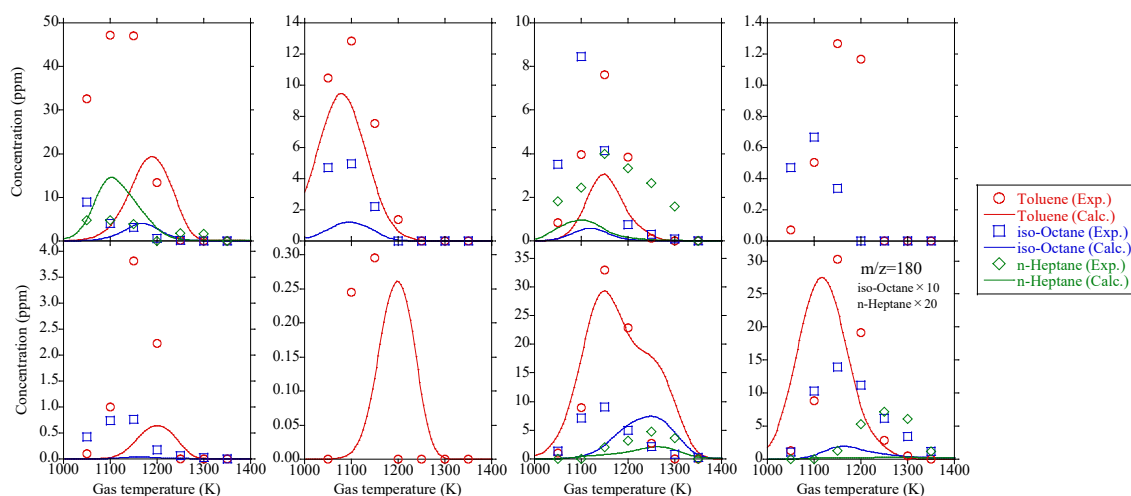


Fig. 4 Concentration profiles of PAHs corresponding to $m/z = 94, 108, 118, 132, 144, 158, 168,$ and 180 in fuel-rich oxidation of toluene, iso-octane, and n-heptane as a function of temperature. Equivalence ratio and residence time were 9.0 and 1.2 s, respectively. Symbols are experimental data; lines are simulated profiles. See Table S3 for structures associated with these m/z values. Note that $m/z = 94, 108, 144, 158$ and others include OPAHs.

toluene and n-heptane in case of iso-octane. The simulation could satisfactorily capture the experimental results in every fuel within a factor of 4, although there were slight deviations between them in the peak concentration temperature.

The experimental tendency of Fig. 4 was generally similar with that of Fig. 3. Note that measured concentrations of several PAHs in iso-octane and n-heptane fuels are not shown in Fig. 4 because they were lower than the detection limit. The mole fractions of minor PAHs in Fig. 4 were much lower than those of major PAHs in Fig. 3. Minor PAHs here include OPAHs, such as $m/z = 94, 108, 144, 158,$ and others, and production of OPAHs was much lower than that of PAHs as observed in previous studies [24,32]. Thus, the difference of concentration between Figs. 3 and 4 seems reasonable.

5.2. Analysis on reactions pathways of PAHs

5.2.1. Major PAHs ($m/z = 78, 92, 104, 116, 128, 152, 154, 166, \text{ and } 178$)

Because the calculated results were generally in good agreement with the experimental data, the present model can be regarded as a reliable one, and the kinetic analysis was carried out using the model. In this section, the detailed analyzed results of naphthalene, acenaphthylene, and phenanthrene, are presented as a representative of PAHs, and those of other aromatics/PAHs are described briefly.

The major aromatic/PAH formation pathways are now described starting with the lowest m/z value of 78 (benzene as shown in Table S3). In toluene fuel at 1250 K, the main benzene formation pathways are ipso-replacement reaction of toluene by H to form benzene ($\text{C}_6\text{H}_5\text{CH}_3 + \text{H} = \text{C}_6\text{H}_6 + \text{CH}_3$) and H elimination of 2,4-cyclohexadienyl radical ($\text{CYC}_6\text{H}_7 = \text{C}_6\text{H}_6 + \text{H}$) which is produced from ring-expansion of 2,4-cyclopentadienylmethyl radical ($\text{C}_5\text{H}_5\text{CH}_2$) formed by CO loss of the cresoxy radical ($\text{OC}_6\text{H}_4\text{CH}_3$). In iso-octane and n-heptane fuels, H elimination of 2,4-cyclohexadienyl radical is dominant for benzene formation at 1250 K, however, 2,4-cyclohexadienyl radical is formed through isomerization of cyclopentadienylmethyl radical ($\text{C}_5\text{H}_5\text{CH}_2$) produced from recombination of propargyl radicals via fulvene.

The species corresponding to toluene in our model is $m/z = 92$ as shown in Table S3. Thus, the main consumption and production pathways of toluene were examined in toluene and iso-octane/n-heptane fuels, respectively. Toluene is primarily consumed by hydrogen abstraction reactions in case of toluene

fuel, while $C_4H_6 + C_3H_3 = C_6H_5CH_3 + H$ is dominant for toluene production in iso-octane and n-heptane fuels at 1150 K.

The formation pathways of species at $m/z = 104$, namely styrene, were analyzed. In toluene fuel at 1150 K, main formation pathway of styrene is the dissociation reaction of stilbene radical ($C_{14}H_{13} = C_6H_5C_2H_3 + C_6H_5$) which is produced from the recombination of benzyl radicals to form bibenzyl ($C_{14}H_{14}$), followed by hydrogen abstraction. On the other hand, styrene is mainly produced through H-assisted isomerization of 5-allylidencyclopenta-1,3-diene (C_5H_4VCCVC) produced from the combination of cyclopentadienyl and propargyl radicals via $C_5H_5C_3H_3$ formation in iso-octane and n-heptane fuels.

Because there are several potential isomers corresponding to $m/z = 116$ as shown in Table S3, comparison of the simulated mole fractions of different isomers is shown in Fig. S5 in the supplementary material. Figure S5 shows that most of mole fractions at $m/z = 116$ is accounted by indene and contribution of other isomers is limited in every fuel studied here. Hence, we investigated the main formation pathways of indene at 1200 K, showing that indene was primarily produced from HACA (hydrogen abstraction carbon addition) pathway ($C_6H_5CH_2 + C_2H_2 = IND + H$) in every fuel. Benzyl radical is formed by H-abstraction reactions of toluene in toluene fuel, while $C_3H_3 + C_4H_4 = C_6H_5CH_2$ also contributes in iso-octane and n-heptane fuels in addition to H-abstraction reactions.

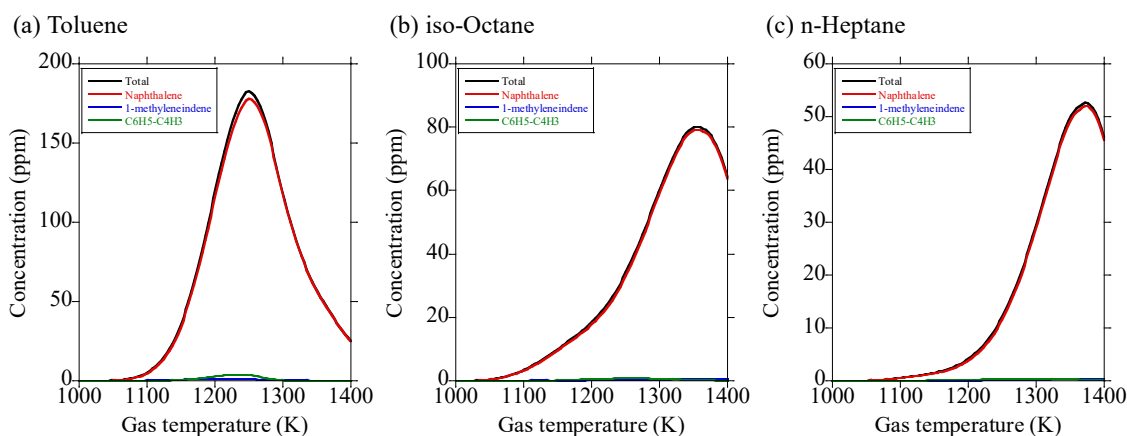


Fig. 5 Comparison of simulated concentrations of different isomers corresponding to $m/z = 128$ in (a) toluene, (b) iso-octane, and (c) n-heptane.

Similarly for $m/z = 128$, there are several possible isomers displayed in Table S3. Among these isomers, naphthalene is the dominant species according to simulations as shown in Fig. 5, thereby the reaction pathways of naphthalene were analyzed in detail. The top 6 reaction pathways toward naphthalene at 1300 K were identified based on rate of production (ROP) analysis: H-assisted isomerization of 1-methyleneindene ($\text{CH}_2\text{IND} + \text{H} = \text{NAPH} + \text{H}$, pathway #1), combination of fulvenallenyl and propargyl radicals ($\text{C}_7\text{H}_5 + \text{C}_3\text{H}_3 \Rightarrow \text{NAPH}$, pathway #2), ring enlargement of methylindene radicals ($\text{C}_9\text{H}_6\text{CH}_3 = \text{NAPH} + \text{H}$ and $\text{C}_9\text{H}_6\text{CH}_3-2 = \text{NAPH} + \text{H}$, pathway #3), H-elimination of dialin radical ($\text{C}_{10}\text{H}_9 \Rightarrow \text{H} + \text{NAPH}$, pathway #4) etc. Figure 6 (a) and (b) show the reaction network and relative contribution of each pathway, respectively. Note that contribution of pathway #4 was sum of $\text{C}_{10}\text{H}_9 \Rightarrow \text{H} + \text{NAPH}$ and $\text{C}_{10}\text{H}_{10} = \text{H}_2 + \text{NAPH}$. The dominant formation pathway of naphthalene depends on the fuels. In toluene, pathway #4 is dominant, followed by pathway #1. The importance of pathway #4 for naphthalene production was also highlighted in another

study when toluene was used as fuel [40]. In case of iso-octane, contribution of pathway #1 is the largest, followed by pathways #4, #3, and #2. n-Heptane fuel shows similar reaction pathways with iso-octane, but the contribution ranks in the order of pathway #1, #2, #3, and #4. The tendency that

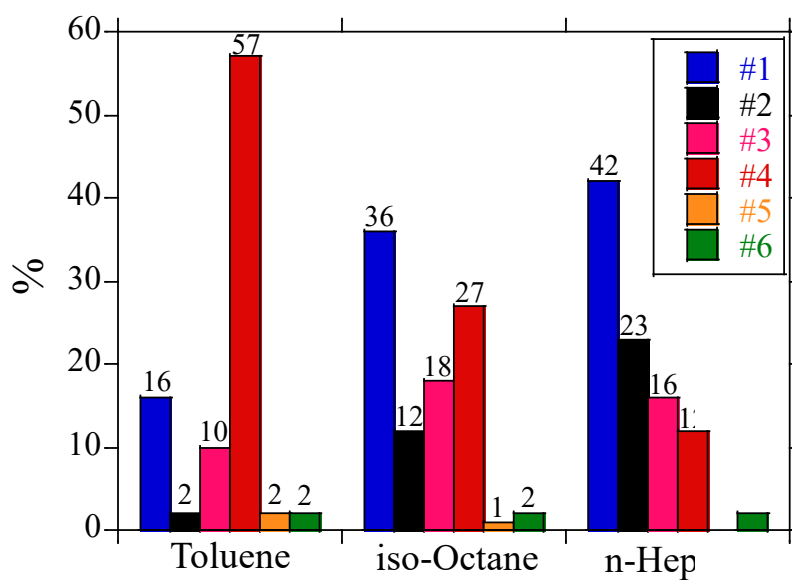
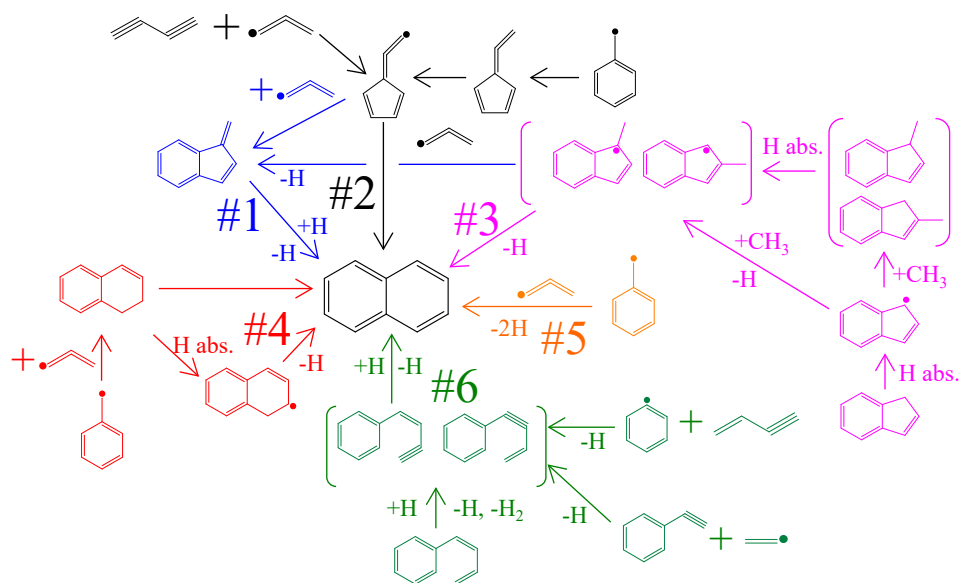


Fig. 6 (a) main reaction pathways for naphthalene formation at 1300 K. (b) relative contribution of each pathway in toluene, iso-octane, and n-heptane fuels.

naphthalene formation is governed by pathways #1, #2, and #3 in normal and branched alkanes was seen in previous studies fuelled by PRFs and n-decane [15,32]. In every fuel, contribution of pathways #5 and #6 is limited. Although pathways #1 and #2 contribute considerably to naphthalene production in every fuel and fulvenallenyl radical (C_7H_5) plays an important role in both pathways, C_7H_5 is primarily produced through sequential hydrogen elimination of benzyl radical in toluene fuel, while it is mainly generated by the reaction between diacetylene (C_4H_2) and propargyl radical in iso-octane and n-heptane fuels. The top 10 reactions contributing to naphthalene production used for calculating the relative contribution in Fig. 6 (b) are given in Fig. S8 in the supplementary material. The largest ROP reaction in toluene fuel is approximately one order of magnitude greater than that in iso-octane which is several times bigger than that in n-heptane. Sensitivity analysis toward naphthalene formation was conducted and top 10 reactions with highest positive coefficient are presented in Fig. 7.

The reactions with positive sensitivity indicate that an increase in the reaction rate enlarges naphthalene production. In toluene fuel, dialin ($C_{10}H_{10}$) formation reaction ($C_3H_3 + C_6H_5CH_2 \Rightarrow C_{10}H_{10}$) as well as H-elimination reactions of 1-methylindene ($C_9H_7CH_3 = C_9H_6CH_3 + H$) and indene ($IND + H = C_9H_7 + H_2$) which appear in pathways #4 and #3 in Fig. 6 (a), respectively, show large positive coefficient. In addition, the reactions involving 2-methylcyclopenta-2,4-dien-1-one ($C_5H_3O-CH_3$) as well as the reactions involving C_5H_5 radical ($C_2H_2 + C_3H_3 = C_5H_5$ and $C_6H_5 + O_2 = C_6H_5O + O$ where C_6H_5O results in C_5H_5 formation via CO removal) show large positive coefficients because

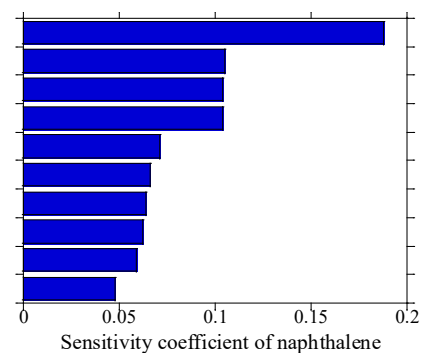
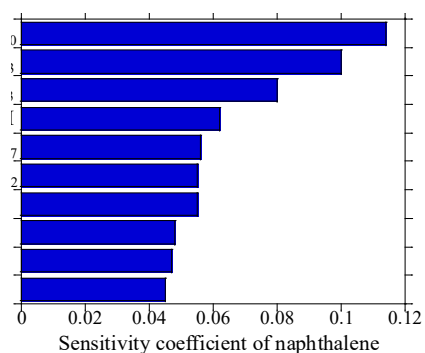
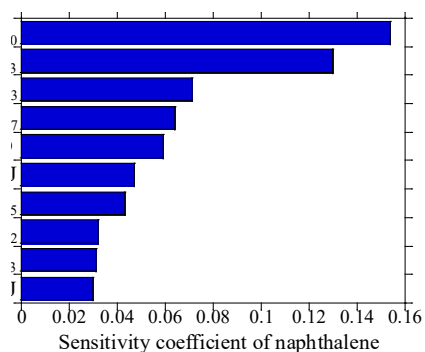


Fig. 7 Sensitivity analysis toward naphthalene formation in (a) toluene, (b) iso-octane, and (c) n-heptane fuels.

these reactions lead to the formation of C_3H_3 which is a significant species for naphthalene formation as shown in Fig. 6 (a). Also, the sensitivity of the reactions involving toluene ($H + C_6H_5CH_3 = H_2 + C_6H_5CH_2$ and $OH + C_6H_5CH_3 = H_2O + C_6H_4CH_3$) cannot be ignored, which is in line with previous study [4,32]. In case of iso-octane, the molecular growth reactions ($C_3H_3 + C_6H_5CH_2 \Rightarrow C_{10}H_{10}$) and H-elimination of 1-methylindene ($C_9H_7CH_3 = C_9H_6CH_3 + H$) which are similar reactions seen in

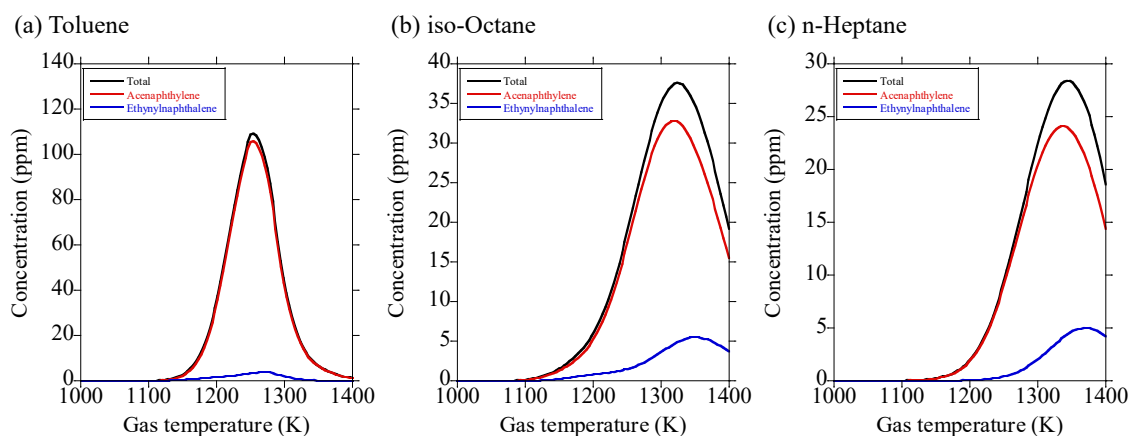


Fig. 8 Comparison of simulated concentrations of different isomers corresponding to $m/z = 152$ in (a) toluene, (b) iso-octane, and (c) n-heptane.

toluene fuel have large positive coefficients. At the same time, the reactions involving C_2 – C_4 species, many of which are correlated with C_3H_3 formation, as well as the aromatic formation reactions from small hydrocarbons (forward direction of $C_3H_3 + C_4H_4 = C_6H_5CH_2$ and $C_3H_3 + C_4H_6 = H + C_6H_5CH_3$) show high sensitivity. In n-heptane, similarly to iso-octane, the reactions involving C_2 – C_4 species, such as $H + C_2H_4 = H_2 + C_2H_3$, $H + C_3H_4-P = H_2 + C_3H_3$, and $C_2H + C_2H_2 = H + C_4H_2$, have large positive coefficients. The molecular growth reactions, such as $C_3H_3 + C_7H_5 = CH_2IND$ and $C_3H_3 + C_7H_5 \Rightarrow NAPH$, and ring formation reaction, such as $C_7H_5 = C_3H_3 + C_4H_2$, which can be found in pathways #1 and #2 in Fig. 6 (a), are present as large sensitivity reactions, while the sensitivity of reactions seen in toluene and iso-octane ($C_3H_3 + C_6H_5CH_2 \Rightarrow C_{10}H_{10}$ and $C_9H_7CH_3 = C_9H_6CH_3 + H$) is relatively low.

The isomers at $m/z = 152$ contained in our model are acenaphthylene, 1-ethynyl naphthalene, and 2-ethynyl naphthalene. Among these species, acenaphthylene accounted for large portion of

concentrations in every fuel as given in Fig. 8, hence, the reaction pathways of acenaphthylene were investigated in detail. Top 4 contributable reaction pathways toward acenaphthylene (A2R5) at 1300 K are depicted in Fig. 9 (a): combination of indenyl and propargyl radicals ($C_9H_7 + C_3H_3 \Rightarrow A2R5 + 2H$, pathway #7), HACA reaction of 1-naphthyl radical (NAPH + $C_2H_2 \Rightarrow A2R5 + H$, pathway #8),

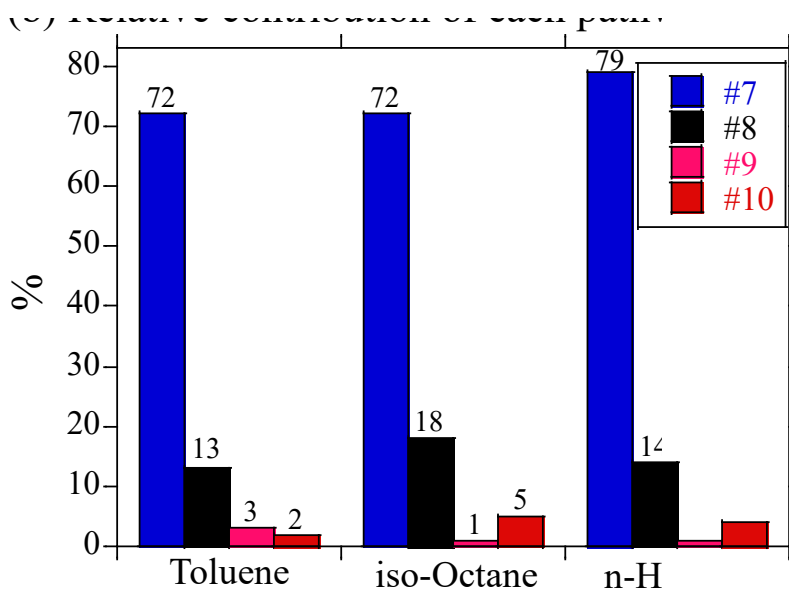
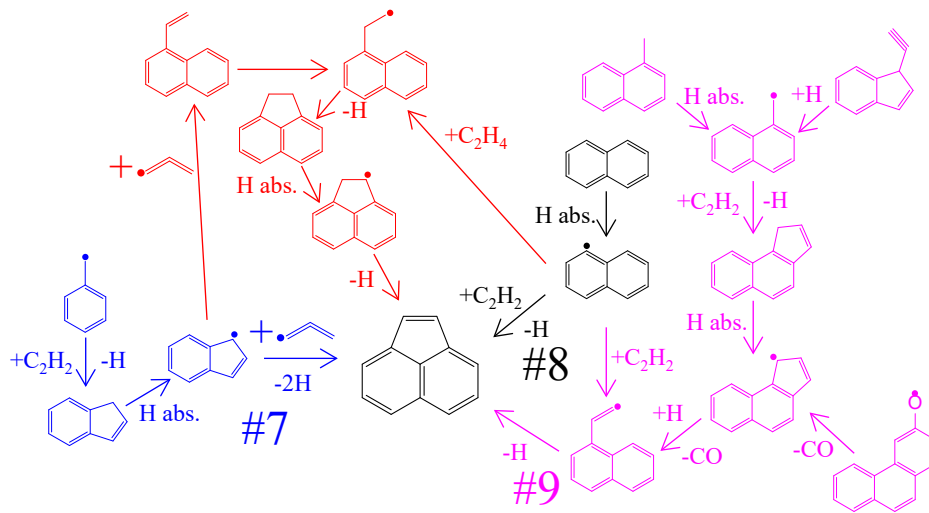


Fig. 9 (a) main reaction pathways for acenaphthylene formation at 1300 K. (b) relative contribution of each pathway in toluene, iso-octane, and n-heptane fuels.

ring closure of vinyl naphthyl radical ($A2C_2H_2 = A2R5 + H$, pathway #9), and sequential H-elimination to form acenaphthene ($RDIHYDROA2R5 = A2R5 + H$, pathway #10). Contribution of these pathways in each fuel are depicted in Fig. 9 (b). Differently from naphthalene, acenaphthylene production is independent on the fuels: pathway #7 dominates, followed by pathway #8, and contribution of other pathways are limited. On the other hand, according to the reactions with large ROP toward

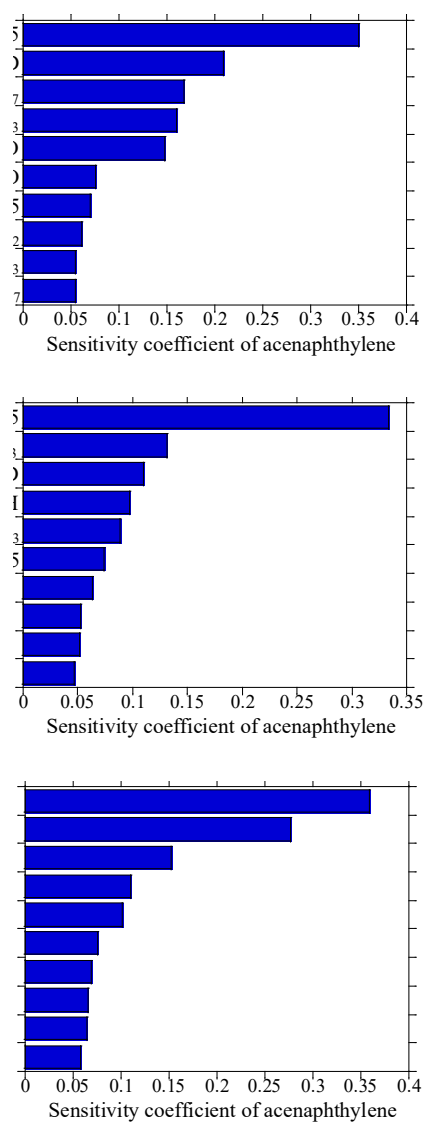


Fig. 10 Sensitivity analysis toward acenaphthylene formation in (a) toluene, (b) iso-octane, and (c) n-heptane fuels.

acenaphthylene production shown in Fig. S9 in the supplementary material, the ranking of ROP is toluene, iso-octane, and n-heptane, which is similar tendency to naphthalene. The results of sensitivity analysis for acenaphthylene are presented in Fig. 10. It is intriguing to note that several molecular growth reactions, such as $C_3H_3 + C_9H_7 \Rightarrow A2R5 + 2H$ and $C_2H_2 + C_6H_5CH_2 = H + IND$, which appear in pathway #7 in Fig. 9 (a), are commonly found as large sensitivity reactions in every fuel. Compared to these reactions, HACA pathway, $C_2H_2 + NAPH- \Rightarrow H + A2R5$, is less influential. Although the reactions correlated to C_2H_2 and C_3H_3 production show large coefficients, the elemental reactions differ depending on the fuels: toluene fuel shows aromatic ring contraction and cleavage, such as $O_2 + C_6H_4CH_3 = HCO + C_5H_3O-CH_3$, $O_2 + C_6H_5 = HCO + C_5H_4O$, and $C_5H_4O \Rightarrow CO + 2C_2H_2$, while iso-octane and n-heptane fuels show H-abstraction reactions, such as $H + C_3H_4-P = H_2 + C_3H_3$, $H + C_2H_4 = H_2 + C_2H_3$, and $H + C_3H_4-A = H_2 + C_3H_3$. As well as naphthalene, it was found that the ring formation reaction from small intermediate species, $C_3H_3 + C_4H_4 = C_6H_5CH_2$, is influential in iso-octane and n-heptane fuels.

There are several potential isomers corresponding to $m/z = 154$ as presented in Table S3, and comparison of the simulated concentrations of different isomers is shown in Fig. S6 in the supplementary material, showing that biphenyl is dominant species in every fuel. According to ROP analysis, the main formation pathway of biphenyl at 1250 K is $C_7H_5 + C_5H_5 \Rightarrow C_{12}H_{10}$ in every fuel. In addition to this, $C_6H_5CH_3 + C_6H_5 = C_{12}H_{10} + CH_3$ is important in toluene fuel.

Although a number of isomers at $m/z = 166$ are included in our model as shown in Table S3, the calculated results in Fig. S7 shows that fluorene is predominant species in every fuel. Thus, this study explores the main formation pathways of fluorene at 1300 K. In toluene fuel, ring-closure reactions involving diphenylmethane radical ($C_6H_5CHC_6H_5 \Rightarrow FLUORENE + H$) and methyl-biphenyl radical ($C_{12}H_9CH_2 = FLUORENE + H$) primarily contribute to fluorene production. In addition to these reactions, $C_7H_5 + C_6H_6 = FLUORENE + H$ and hydrogenation of fluorenyl radical are important in iso-octane and n-heptane fuels. Fluorenyl radical is produced from CO elimination of oxygenated phenanthrene radical (PHNTHRNOJ \Rightarrow RFLUORENE + CO) and benzo-fulvenallenyl radical + acetylene ($C_9H_6-C_2H + C_2H_2 = RFLUORENE$) in iso-octane and n-heptane, respectively. Although phenalene formation reaction from methyl-naphthyl radical (A2CH₂) is suggested to be important in production of PAH at $m/z = 166$ in α -methyl-naphthalene pyrolysis [41], this pathway is not important in the present mechanism.

Chemical species at $m/z = 178$ contains several isomers as shown in Table S3. Among these species, phenanthrene accounts for a considerable portion of the simulated mole fractions at $m/z = 178$ in Fig. 11. Although diphenylacetylene accounts for unignorable amounts at $m/z = 178$, it is adequate to examine the main reaction pathway of phenanthrene based on ROP analysis because it becomes a precursor of phenanthrene as will be explained later. Fig. 12 (a) illustrates the main formation pathway of phenanthrene at 1300 K: H-assisted isomerization of diphenylacetylene and H-loss of stilbene

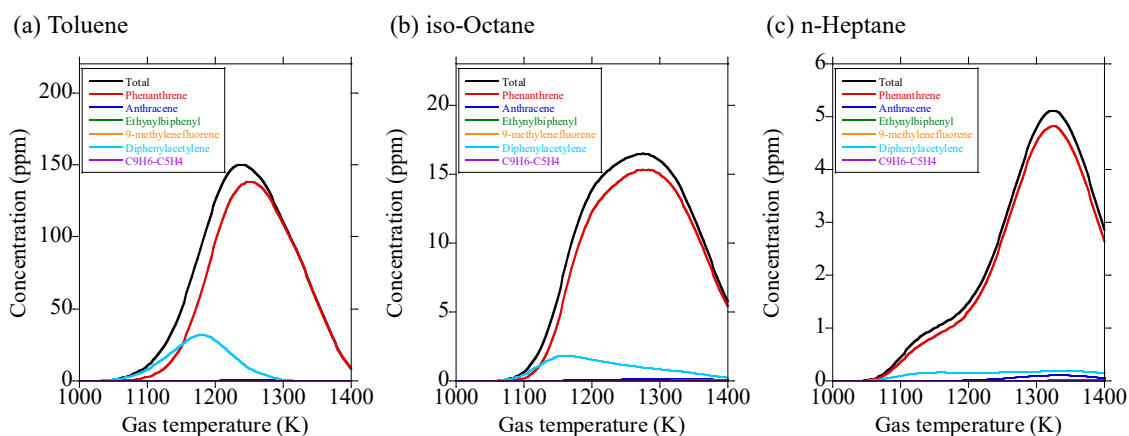


Fig. 11 Comparison of simulated concentrations of different isomers corresponding to $m/z = 178$ in (a) toluene, (b) iso-octane, and (c) n-heptane.

radical ($H + C_6H_5C_2C_6H_5 = H + PHNTHRN$ and $C_{14}H_{11} = H + PHNTHRN$, pathway #11), H-assisted isomerization of 9-methylene fluorene ($H + CH_2FLUORENE \Rightarrow H + PHNTHRN$, pathway #12), HACA pathway from biphenyl ($C_2H_2 + C_{12}H_9 \Rightarrow H + PHNTHRN$, pathway #13), ring enlargement of methyl-benzoindenyl radical ($RMEA2CYC5 \Rightarrow H + PHNTHRN$, pathway #14), combination of benzo-fulvenallenyl and propargyl radicals ($C_3H_3 + C_9H_6-C_2H \Rightarrow PHNTHRN$, pathway #15), and recombination of fulvenallenyl radicals ($2C_7H_5 \Rightarrow PHNTHRN$, pathway #16). Although pathway #11 is the most important toward phenanthrene production in every fuel as shown in Fig. 12 (b), contribution of other pathways depends on the fuels. Pathway #12 is second contributable pathway for phenanthrene formation in toluene fuel, whereas pathways #13 and #14 are contributable to some degree in iso-octane fuel. In case of n-heptane, pathway #15 contributes to phenanthrene production subsequently to pathway #11, followed by pathways #13 and #14. Although a previous study emphasized the importance of benzo-fulvenallenyl radical in PAH formation [41], its contribution to

PAHs up to three ring structure that were measured in this study was limited. Because there are limited studies on the reaction chemistry of benzo-fulvenallenyl radical at present, further investigations

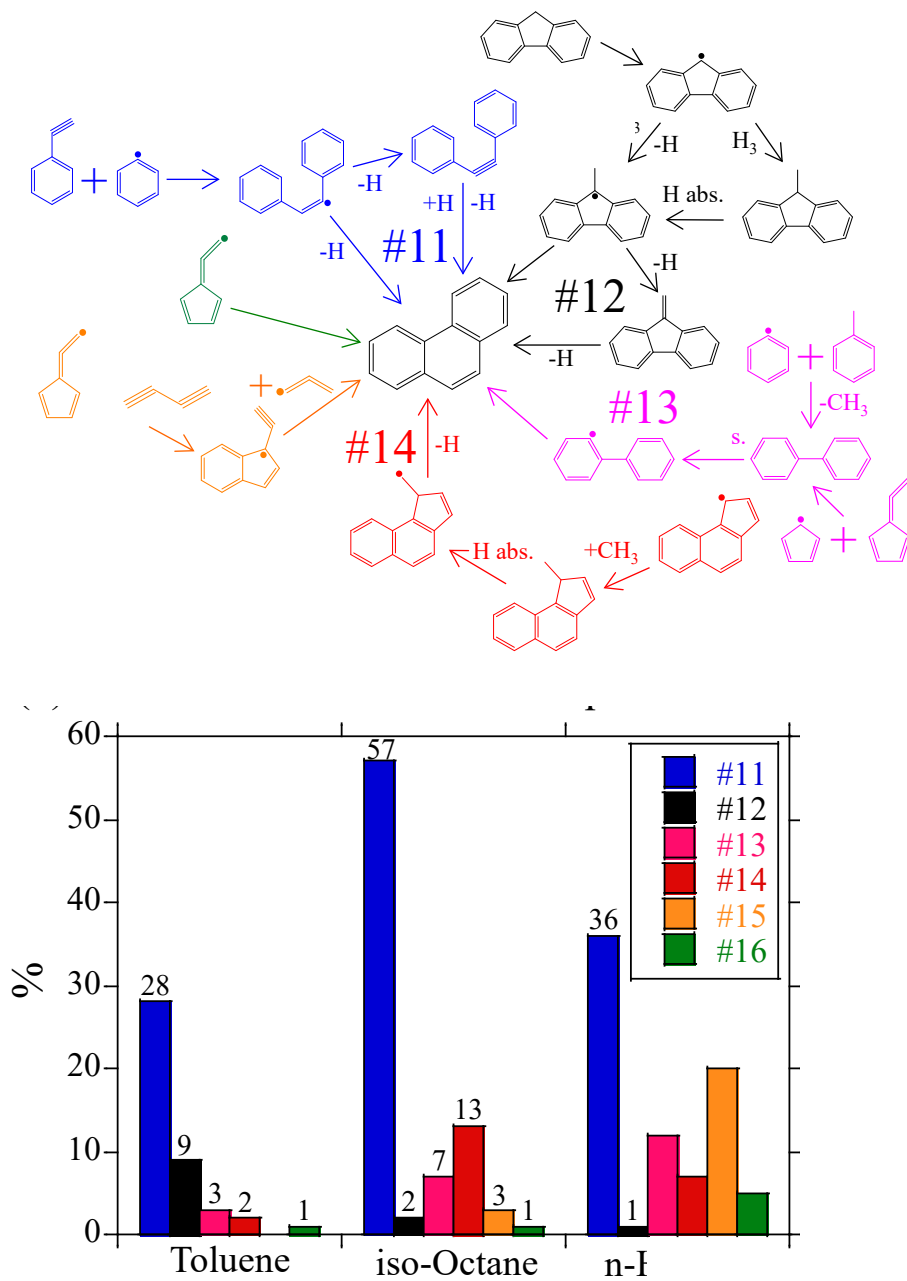


Fig. 12 (a) main reaction pathways for phenanthrene formation at 1300 K. (b) relative contribution of each pathway in toluene, iso-octane, and n-heptane fuels.

should be carried out in the future to refine the reaction mechanism involving benzo-fulvenallenyl radical. On the other hand, as suggested by the previous paper [41], benzo-fulvenallenyl radical may play a crucial role in the formation of larger PAHs than those measured in this study. The integrated ROP of phenanthrene shown in Fig. S10 in the supplementary material indicates that the order of phenanthrene ROP is toluene, iso-octane, and n-heptane, which is similar tendency to naphthalene and acenaphthylene. The sensitivity analysis toward phenanthrene production is shown in Fig. 13. In every fuel, the reactions appearing in pathway #11 in Fig. 12 (a), such as $C_{14}H_{11} = C_6H_5 + C_6H_5C_2H$ and $H + C_6H_5C_2C_6H_5 = H + PHNTHRN$, have large positive coefficients. This result is consistent with that of Fig. 12 (b) where pathway #11 is dominant for phenanthrene in every fuel. In n-heptane, note that the reactions related to pathway #15 important only in n-heptane, such as $C_9H_6-C_2H = C_4H_2 + C_7H_5$ and $C_7H_5 = C_3H_3 + C_4H_2$, show large sensitivity. As well as naphthalene and acenaphthylene, in iso-octane and n-heptane, there are several reactions with large sensitivity which involve small species, such as $H + C_3H_4-P = H_2 + C_3H_3$, $H + C_2H_4 = H_2 + C_2H_3$, and others, while the reactions involving toluene, such as $O_2 + C_6H_5CH_3 = HO_2 + C_6H_5CH_2$ and $H + C_6H_5CH_3 = CH_3 + C_6H_6$, are influential in toluene fuel. To summarize the sensitivity analysis of naphthalene, acenaphthylene, and phenanthrene, the molecular growth reactions with high sensitivity are relatively common in every fuel once aromatic species which becomes origin of PAH growth reactions are formed. In iso-octane and n-heptane, the

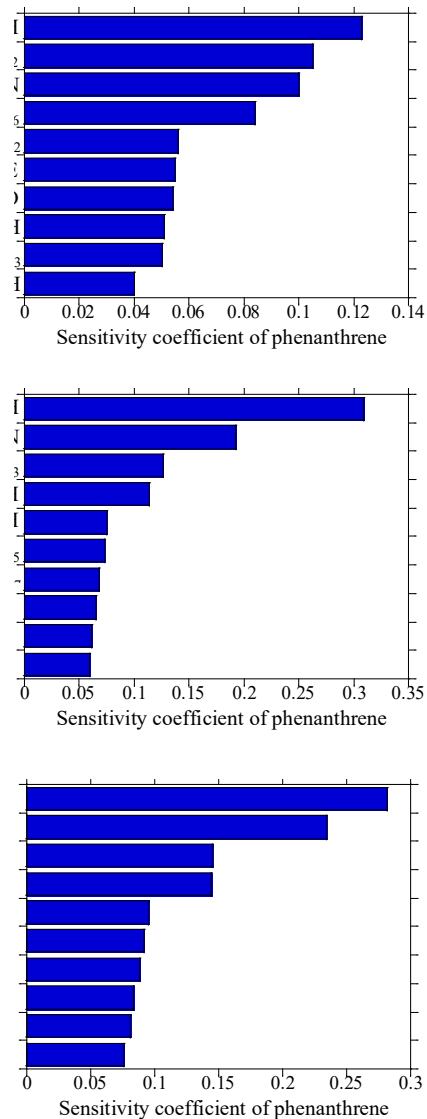


Fig. 13 Sensitivity analysis toward phenanthrene formation in (a) toluene, (b) iso-octane, and (c) n-heptane fuels.

ring formation reactions from small species are found as high sensitivity reactions because aromatic ring is absent in their molecular structure, while the reactions involving toluene are influential in toluene fuel because toluene reactivity is much lower than iso-octane and n-heptane. It was also common between the fuels that the reactions leading to C_2H_2 and C_3H_3 which are important in the reactions of molecular growth and ring formation have large positive coefficients, but the reaction

pathways depend on the fuels: they can be produced through ring contraction and cleavage in toluene fuel, while they are formed by the reactions involving small species in iso-octane and n-heptane.

5.2.2. Minor PAHs ($m/z = 108, 118, 158, \text{ and } 168$)

For the kinetic analysis of minor PAHs, only several m/z were selected for discussion because of relatively good agreement between the experimental and simulated results. We adopted the signal at $m/z = 108, 118, 158, \text{ and } 168$, and these signals include OPAHs in addition to PAHs. It is important to examine whether PAHs or OPAHs are the predominant species. Furthermore, because there are limited studies on the reaction pathways of OPAHs, it is important to reveal them by kinetic analysis.

Starting with $m/z = 108$, calculated mole fractions of several species are given in Fig. S11 in the supplementary material, showing that cresol is the dominant species in toluene and iso-octane fuels. Note that the experimental data for $m/z = 108$ in n-heptane is lower than the detection limit, thereby simulated result in n-heptane is not plotted in Fig. S11. Because the calculation showed that the maximum concentration at $m/z = 108$ in n-heptane was below 0.06 ppm, which is lower than the detection limit in the present analysis equipment, the experimental results seem reasonable. In both fuels, cresol is directly produced from toluene ($\text{C}_6\text{H}_5\text{CH}_3 + \text{O} = \text{HOC}_6\text{H}_4\text{CH}_3$) at 1100 K according to ROP analysis.

At $m/z = 118$, Fig. S12 shows that simulated concentrations of allylbenzene ($\text{C}_6\text{H}_5\text{C}_3\text{H}_5\text{-1}$) are

dominant over those of benzofuran in every fuel. $C_6H_5CH_2 + C_2H_3 = C_6H_5C_3H_5-1$ is a predominant reaction toward allylbenzene formation in toluene fuel at 1100 K. In iso-octane fuel, $C_6H_5 + C_3H_5-A = C_6H_5C_3H_5-1$ and $C_6H_5 + C_3H_6 = C_6H_5C_3H_5-1 + H$ are important, while $C_6H_5CH_2 + C_2H_3 = C_6H_5C_3H_5-1$ and $C_6H_5 + C_3H_5-A = C_6H_5C_3H_5-1$ are dominant in n-heptane.

The signal attributed to $m/z = 158$ was detected only in toluene fuel, and comparison of the simulated mole fractions of several species is presented in Fig. S13 where 1,4-naphthoquinone (P-OA2O) is dominant. 1,4-naphthoquinone is primarily produced through $NAPH- + O_2 = P-OA2O + H$.

Species corresponding to $m/z = 168$ includes PAHs ($C_6H_5CH_2C_6H_5$, ME-C₁₂H₉, ALLYLNAPH-1, and ALLYLNAPH-2) and OPAH (DBZFUR) as shown in Table S3. According to the calculation, the dominant species depends on the temperature in toluene fuel, while dibenzofuran (DBZFUR) is the main product in iso-octane and n-heptane fuels. In toluene at around 1150 K, diphenylmethane ($C_6H_5CH_2C_6H_5$) and methylbiphenyl (ME-C₁₂H₉) are dominant over dibenzofuran. The main formation reaction of diphenylmethane is combination of phenyl and benzyl radicals ($C_6H_5CH_2 + C_6H_5 = C_6H_5CH_2C_6H_5$) and methylbiphenyl is dominantly produced via reactions involving monoaromatic species ($C_6H_5CH_3 + C_6H_4CH_3 = ME-C_{12}H_9 + CH_3$ and $C_6H_5CH_3 + C_6H_5 = ME-C_{12}H_9 + H$). When a temperature increases, the dominant species changes to dibenzofuran instead of aforementioned species in toluene fuel. The main production pathway of dibenzofuran in toluene fuel at 1250 K involves cyclization of C₁₂H₉O (C₁₂H₉O = RDHYDRODBZFUR1) which is produced through oxygen

addition to biphenyl radical, subsequently undergoing dehydrogenation ($\text{RDHYDRODBZFUR1} = \text{DBZFUR} + \text{H}$). The main formation pathway of dibenzofuran in iso-octane and n-heptane is similar to that in toluene. The tendency that the primary production pathway of OPAH is independent on the fuels is consistent with previous study [32].

6. CONCLUSIONS

The fuel-rich oxidation of gasoline surrogate components like toluene, iso-octane, and n-heptane was studied using an atmospheric-pressure flow reactor at temperatures from 1050 to 1350 K, residence times of 0.45 and 1.2 s, and equivalence ratio of 9.0. In addition to PAHs from one to three ring structure, small intermediate species of $\text{C}_1\text{--C}_5$ produced during oxidation of the fuels were quantified. The kinetic model which was originally developed by LLNL was refined in terms of PAH growth reactions. In general, the revised model could satisfactorily capture the experimental results of small intermediate products as well as many PAHs. The experimental and simulated results showed that the mole fractions of small intermediate species were affected by the fuels, while production of PAHs was in the order of toluene, iso-octane, and n-heptane. To investigate the PAH formation pathways of three fuels, the kinetic analysis using the updated model was conducted. We investigated the formation pathways of major and minor PAHs, particularly focusing on naphthalene, acenaphthylene, and phenanthrene. According to ROP analysis, the main production pathways of naphthalene and

phenanthrene were affected by the fuels, while they were nearly independent on them for the production of acenaphthylene. Although the resonantly stabilized radicals, such as benzyl and fulvenallenyl radicals, served an important role in PAH growth reactions in every fuel, their main formation pathways depended on the fuels. Sensitivity analysis showed that there were common reactions with large sensitivity among every fuel, such as the molecular growth reactions and reactions leading to production of small species which behaved as key building blocks in PAH growth. In addition, the reactions to form aromatic rings from small species showed large sensitivity coefficients in iso-octane and n-heptane, while those involving toluene had relatively large coefficients in toluene. These results obtained in this study that the main formation pathways of PAHs and the influential reactions toward PAH production were affected by the fuels could be helpful in understanding the reaction chemistry of PAHs in the fuel rich oxidation of gasoline surrogate components.

Declaration of Competing Interest

There is no known competing financial interests or personal relationships that influence the work reported in this paper.

Acknowledgements

This research was financially supported by the Environment Research and Technology Development Fund (JPMEERF20205R04) of the Environmental Restoration and Conservation Agency of Japan and SUZUKI FOUNDATION. The authors convey their special thanks to a former researcher at LLNL, Dr. Goutham Kukkadapu. Research at LLNL was performed under the auspices of the U.S. Department of Energy (DOE) by Lawrence Livermore National Laboratory under Contract DE-AC52-07NA27344.

REFERENCES

- ¹ M. Heal, P. Kumar, R. Harrison, Particles, air quality, policy and health, *Chem. Soc. Rev.*, 41 (2012) 6606–6630.
- ² C. Myung, S. Park, Exhaust nanoparticle emissions from internal combustion engines: A review, *Int. J. Autom. Technol.* 13 (2012) 9–22.
- ³ Y. Wang, S.H. Chung, Soot formation in laminar counterflow flames, *Prog. Energy Combust. Sci.* 74 (2019) 152–238.
- ⁴ S. Suzuki, G. Kukkadapu, Y. Ishii, T. Katsumi, K. Kinoshita, Y. Takeda, S. Sakaida, M. Konno, Y. Sakai, K. Tanaka, M. Oguma, W.J. Pitz, Blending Effect of Methanol on the Formation of Polycyclic Aromatic Hydrocarbons in the Oxidation of Toluene, *Proc. Combust. Inst.* In Press (2022)
- ⁵ S.M. Sarathy, A. Farooq, G.T. Kalghatgi, Recent progress in gasoline surrogate fuels, *Prog. Energy Combust. Sci.* 65 (2018) 67–108.
- ⁶ H. Chu, L. Xiang, X. Nie, Y. Ya, M. Gu, J. E, Laminar burning velocity and pollutant emissions of the gasoline components and its surrogate fuels: A review, *Fuel* 269 (2020) 117451.
- ⁷ P. Dirrenberger, P.A. Glaude, R. Bounaceur, H. Le Gall, A. Pires da Cruz, A.A. Konnov, F. Battin-Leclerc, Laminar burning velocity of gasolines with addition of ethanol, *Fuel* 115 (2014) 162–169.
- ⁸ T. Javed, C. Lee, M. AlAbbad, K. Djebbi, M. Beshir, J. Badra, H. Curran, A. Farooq, Ignition studies of n-heptane/iso-octane/toluene blends, *Combust. Flame* 171 (2016) 223–233.
- ⁹ B.C. Choi, S.K. Choi, S.H. Chung, Soot formation characteristics of gasoline surrogate fuels in counterflow diffusion flames, *Proc. Combust. Inst.* 33 (2011) 609–616.
- ¹⁰ S. Park, Y. Wang, S.H. Chung, S.M. Sarathy, Compositional effects on PAH and soot formation in counterflow diffusion flames of gasoline surrogate fuels, *Combust. Flame* 178 (2017) 46–60.
- ¹¹ Y. Hua, F. Liu, H. Wu, C. Lee, Z. Wang, Experimental Evaluation of Various Gasoline Surrogates Based on Soot Formation Characteristics, *Energy Fuels* 32 (2018) 11961–11969.
- ¹² S. Liang, Z. Li, J. Gao, X. Ma, H. Xu, S. Shuai, PAHs and soot formation in laminar partially premixed co-flow flames fuelled by PRFs at elevated pressures, *Combust. Flame* 206 (2019) 363–378.
- ¹³ S. Kruse, A. Wick, P. Medwell, A. Attili, J. Beeckmann, H. Pitsch, Experimental and numerical study of soot formation in counterflow diffusion flames of gasoline surrogate components, *Combust. Flame* 210 (2019) 159–171.
- ¹⁴ C. Shao, H. Wang, N. Atef, Z. Wang, B. Chen, M. Almalki, Y. Zhang, C. Cao, J. Yang, S.M. Sarathy, Polycyclic aromatic hydrocarbons in pyrolysis of gasoline surrogates (n-heptane/iso-octane/toluene), *Proc. Combust. Inst.* 37 (2019) 993–1001.
- ¹⁵ C. Shao, G. Kukkadapu, S.W. Wagnon, W.J. Pitz, S.M. Sarathy, PAH formation from jet stirred reactor pyrolysis of gasoline surrogates, *Combust. Flame* 219 (2020) 312–326.
- ¹⁶ D.S.N. Parker, R.I. Kaiser, T.P. Troy, M. Ahmed, Hydrogen abstraction/acetylene addition revealed, *Angew. Chem. Int. Ed.* 53 (2014) 7740–7744.
- ¹⁷ D.P. Porfiriev, V.N. Azyazov, A.M. Mebel, Conversion of acenaphthalene to phenalene via methylation: A theoretical study, *Combust. Flame* 213 (2020) 302–313.
- ¹⁸ H. Jin, L. Xing, D. Liu, J. Hao, J. Yang, A. Farooq, First aromatic ring formation by the radical-chain reaction of vinylacetylene and propargyl, *Combust. Flame* 225 (2021) 524–534.
- ¹⁹ S. Suzuki, A. Obuchi, G. Kukkadapu, K. Kinoshita, Y. Takeda, M. Oguma, K. Tanaka, W.J. Pitz, Measurements of Intermediate Species in Fuel-rich Oxidation of Ethylene, Toluene, and n-Decane, *Energy Fuels* 35 (2021) 14924–14940.
- ²⁰ G. Kukkadapu, S.W. Wagnon, W.J. Pitz, N. Hansen, Identification of the molecular-weight growth reaction network in counterflow flames of the C₃H₄ isomers allene and propyne, *Proc. Combust. Inst.* 38 (2021) 1477–1485.
- ²¹ F.N. Eglfopoulos, N. Hansen, Y. Ju, K. Kohse-Höinghaus, C.K. Law, F. Qi, Advances and challenges in laminar flame experiments and implications for combustion chemistry, *Prog. Energy Combust. Sci.* 43 (2014) 36–67.
- ²² W. Yuan, T. Li, Y. Li, M. Zeng, Y. Zhang, J. Zou, C. Cao, W. Li, J. Yang, F. Qi, Experimental and kinetic modeling investigation on anisole pyrolysis: Implications on phenoxy and cyclopentadienyl

chemistry, *Combust. Flame* 201 (2019) 187–199.

²³ M. Schenk, L. Leon, K. Moshhammer, P. Oßwald, T. Zeuch, L. Seidel, F. Mauss, K. Kohse-Höinghaus, Detailed mass spectrometric and modeling study of isomeric butene flames, *Combust. Flame* 160 (2013) 487–503.

²⁴ S. Suzuki, S. Kiuchi, K. Kinoshita, Y. Takeda, S. Sakaida, M. Konno, K. Tanaka, M. Oguma, Formation of polycyclic aromatic hydrocarbons, benzofuran, and dibenzofuran in fuel-rich oxidation of toluene using a flow reactor, *Phys. Chem. Chem. Phys.* 23 (2021) 6509–6525.

²⁵ G. Mallocci, G. Mulas, C. Joblin, Electronic absorption spectra of PAHs up to vacuum UV: Towards a detailed model of interstellar PAH photophysics, *Astron. Astrophys.* 426 (2004) 105–117.

²⁶ T.A. Cool, K. Nakajima, C.A. Taatjes, A. McIlroy, P.R. Westmoreland, M.E. Law, A. Morel, Studies of a fuel-rich propane flame with photoionization mass spectrometry, *Proc. Combust. Inst.* 30 (2005) 1681–1688.

²⁷ Z. Zhou, M. Xie, Z. Wang, F. Qi, Determination of absolute photoionization cross-sections of aromatics and aromatic derivatives, *Rapid Commun. Mass Spectrom.* 23 (2009) 3994–4002.

²⁸ H. Jin, J. Yang, A. Farooq, Determination of absolute photoionization cross-sections of some aromatic hydrocarbons, *Rapid Commun. Mass Spectrom.* 34 (2020) e8899.

²⁹ L. Ruwe, K. Moshhammer, N. Hansen, K. Kohse-Höinghaus, Influences of the molecular fuel structure on combustion reactions towards soot precursors in selected alkane and alkene flames, *Phys. Chem. Chem. Phys.* 20 (2018) 10780–10795.

³⁰ G. Kukkadapu, D. Kang, S.W. Wagnon, K. Zhang, M. Mehl, M. Monge-Palacios, H. Wang, S.S. Goldsborough, C.K. Westbrook, W.J. Pitz, Kinetic modeling study of surrogate components for gasoline, jet and diesel fuels. C7-C11 methylated aromatics, *Proc. Combust. Inst.* 37 (2019) 521–529.

³¹ N. Hansen, B. Yang, M. Braun-Unkhoff, A. Ramirez, G. Kukkadapu, Molecular-growth pathways in premixed flames of benzene and toluene doped with propyne, *Combust. Flame* 243 (2022) 112075.

³² S. Suzuki, G. Kukkadapu, S. Kiuchi, S.W. Wagnon, K. Kinoshita, Y. Takeda, S. Sakaida, M. Konno, K. Tanaka, M. Oguma, W.J. Pitz, Formation of PAHs, phenol, benzofuran, and dibenzofuran in a flow reactor from the oxidation of ethylene, toluene, and n-decane, *Combust. Flame* 241 (2022) 112136.

³³ A. Cuoci, A. Frassoldati, T. Faravelli, E. Ranzi, Numerical Modeling of Laminar Flames with Detailed Kinetics Based on the Operator-Splitting Method, *Energy and Fuels*, 27 (2013) 7730–7753.

³⁴ A. Cuoci, A. Frassoldati, T. Faravelli, E. Ranzi, OpenSMOKE++: An object-oriented framework for the numerical modeling of reactive systems with detailed kinetic mechanisms, *Comput. Phys. Commun.* 192 (2015) 237–264.

³⁵ J. Jones, G.B. Bacskay, J.C. Mackie, Decomposition of the Benzyl Radical: Quantum Chemical and Experimental (Shock Tube) Investigations of Reaction Pathways, *J. Phys. Chem. A* 101 (1997) 7105–7113.

³⁶ H. Wang, E. Dames, B. Sirjean, D.A. Sheen, R. Tango, A. Violi, J.Y. W. Lai, F.N. Egolfopoulos, D.F. Davidson, R.K. Hanson, C.T. Bowman, C.K. Law, W. Tsang, N.P. Cernansky, D.L. Miller, R.P. Lindstedt, A high-temperature chemical kinetic model of n-alkane (up to n-dodecane), cyclohexane, and methyl-, ethyl-, n-propyl and n-butyl-cyclohexane oxidation at high temperatures, *JetSurF* version 2.0, September 19, 2010 (<http://web.stanford.edu/group/haiwanglab/JetSurF/JetSurF2.0/index.html>).

³⁷ G. da Silva, J.A. Cole, J.W. Bozzelli, Kinetics of the Cyclopentadienyl + Acetylene, Fulvenallene + H, and 1-Ethynylcyclopentadiene + H Reactions, *J. Phys. Chem. A* 114 (2010) 2275–2283.

³⁸ D. Trogolo, A. Maranzana, G. Ghigo, G. Tonachini, First Ring Formation by Radical Addition of Propargyl to But-1-ene-3-yne in Combustion. Theoretical Study of the C₇H₇ Radical System, *J. Phys. Chem. A* 118 (2014) 427–440.

³⁹ L. Monluc, A.A. Nikolayev, I.A. Medvedkov, V.N. Azyazov, A.N. Morozov, A.M. Mebel, The Reaction of o-Benzynes with Vinylacetylene: An Unexplored Way to Produce Naphthalene, *ChemPhysChem* 23 (2022) e202100758.

⁴⁰ S. Dong, S.W. Wagnon, L. Pratali Maffei, G. Kukkadapu, A. Nobili, Q. Mao, M. Pelucchi, L. Cai, K. Zhang, M. Raju, T. Chatterjee, W.J. Pitz, T. Faravelli, H. Pitsch, P. Kelly Senecal, H.J. Curran, A new detailed kinetic model for surrogate fuels: C3MechV3.3, *Appl. Energy Combust. Sci.* 9 (2022) 100043.

⁴¹ H. Jin, J. Hao, J. Yang, J. Guo, Y. Zhang, C.C. Cao, A. Farooq, Experimental and kinetic modeling study of α -methyl-naphthalene pyrolysis: Part II. PAH formation, *Combust. Flame* 233 (2021) 111530.

-
- ⁴² H. Jin, L. Xing, J. Hao, J. Yang, Y. Zhang, C.C. Cao, Y. Pan, A. Farooq, A chemical kinetic modeling study of indene pyrolysis, *Combust. Flame* 206 (2019) 1–20.
- ⁴³ A. Hamadi, W. Sun, S. Abid, N. Chaumeix, A. Comandini, An experimental and kinetic modeling study of benzene pyrolysis with C2–C3 unsaturated hydrocarbons, *Combust. Flame* 237 (2022) 111858.
- ⁴⁴ H. Jin, L. Ye, J. Yang, Y. Jiang, L. Zhao, A. Farooq, Inception of Carbonaceous Nanostructures via Hydrogen-Abstraction Phenylacetylene-Addition Mechanism, *J. Am. Chem. Soc.* 143 (2021) 20710–20716.
- ⁴⁵ A. Matsugi, A. Miyoshi, Reactions of o-benzyne with propargyl and benzyl radicals: potential sources of polycyclic aromatic hydrocarbons in combustion, *Phys. Chem. Chem. Phys.* 14 (2012) 9722–9728.
- ⁴⁶ G.R. Galimova, I.A. Medvedkov, A.M. Mebel, The Role of Methylaryl Radicals in the Growth of Polycyclic Aromatic Hydrocarbons: The Formation of Five-Membered Rings, *J. Phys. Chem. A* 126 (2022) 1233–1244.
- ⁴⁷ X. Shi, Q. Wang, A. Violi, Reaction pathways for the formation of five-membered rings onto polyaromatic hydrocarbon framework, *Fuel* 283 (2021) 119023.
- ⁴⁸ F. Hirsch, I. Fischer, S. Bakels, A.M. Rijs, Gas-Phase Infrared Spectra of the C₇H₅ Radical and Its Bimolecular Reaction Products, *J. Phys. Chem. A* 126 (2022) 2532–2540.
- ⁴⁹ L. Zhao, R.I. Kaiser, W. Lu, M. Ahmed, A.D. Oleinikov, V.N. Azyazov, A.M. Mebel, A.H. Howlader, S.F. Wnuk, Gas phase formation of phenalene via 10π-aromatic, resonantly stabilized free radical intermediates, *Phys. Chem. Chem. Phys.* 22 (2020) 15381–15388.
- ⁵⁰ W. Sun, A. Hamadi, S. Abid, N. Chaumeix, A. Comandini, Influences of propylene/propyne addition on toluene pyrolysis in a single-pulse shock tube, *Combust. Flame* 236 (2022) 111799.
- ⁵¹ H. Jin, W. Chen, L. Ye, H. Lou, Q. Xu, B. Feng, Z. Wang, A. Farooq, Reaction kinetics of phenyl + phenylacetylene at combustion-relevant intermediate temperatures, *Combust. Flame* 243 (2022) 112014.
- ⁵² A.M. Mebel, V.V. Kislov, Can the C₅H₅ + C₅H₅ → C₁₀H₁₀ → C₁₀H₉ + H/C₁₀H₈ + H₂ Reaction Produce Naphthalene? An Ab Initio/RRKM Study, *J. Phys. Chem. A* 113 (2009) 9825–9833.
- ⁵³ V.S. Krasnoukhov, M.V. Zagidullin, I.P. Zavershinskiy, A.M. Mebel, Formation of Phenanthrene via Recombination of Indenyl and Cyclopentadienyl Radicals: A Theoretical Study, *J. Phys. Chem. A* 124 (2020) 9933–9941.
- ⁵⁴ A.N. Morozov, I.A. Medvedkov, V.N. Azyazov, A.M. Mebel, Theoretical Study of the Phenoxy Radical Recombination with the O(³P) Atom, Phenyl plus Molecular Oxygen Revisited, *J. Phys. Chem. A* 125 (2021) 3965–3977.
- ⁵⁵ P. Frank, J. Herzler, T. Just, C. Wahl, High-temperature reactions of phenyl oxidation, *Symp. Int. Combust.* 25 (1994) 833–840.
- ⁵⁶ A.R. Ghildina, A.D. Oleinikov, V.N. Azyazov, A.M. Mebel, Reaction mechanism, rate constants, and product yields for unimolecular and H-assisted decomposition of 2,4-cyclopentadienone and oxidation of cyclopentadienyl with atomic oxygen, *Combust. Flame* 183 (2017) 181–193.